INTERNATIONAL JOURNAL FOR NUMERICAL METHODS IN ENGINEERING
*Int. J. Numer. Meth. Engng.* **43**, 493–506 (1998)

# A DESCRIPTION OF MACROSCOPIC DAMAGE THROUGH MICROSTRUCTURAL RELAXATION

T. ZOHDI, M. FEUCHT, D. GROSS AND P. WRIGGERS *

*Institut für Mechanik IV, Technische Universität Darmstadt, Hochschulstrasse1, D-64289 Darmstadt, Germany*

## ABSTRACT

In this paper a flexible model for the description of damage in heterogeneous structural materials is presented. The approach involves solving the equations of equilibrium, with unilateral constraints on the maximum attainable values of selected internal variables. Due to the unilateral constraints, the problem is non-linear. Accordingly, a simple iterative algorithm is developed to solve this problem by (1) computing the internal fields with the initial undamaged microstructure and (2) reducing the material stiffness at locations where the constraints are violated. This process is repeated until a solution, with a corresponding microstructure, that satisfies the equations of equilibrium and the constraints, is found. The corresponding microstructure is the final 'damaged' material. As an application, the method is used in an incremental fashion to generate response curves describing the progressive macroscopic damage for a sample of commonly used fibre-reinforced Aluminum/Boron composite. The results are compared to laboratory experiments published by Kyono *et al.*[1] and computational results using standard numerical methods, published by Brockenbrough *et al.*[2] © 1998 John Wiley & Sons, Ltd.

KEY WORDS: damage; composites; unilateral constraints; finite elements

## 1. INTRODUCTION

As a solid heterogeneous body is subjected to increasing loads, microfailures occur. These may be in the form of microcracks, interface separation, void nucleation, dislocation pile ups, etc. As the loading progresses, these local failures increase in size and number and eventually merge to produce observed macroscopic failure or damage. Alone, the definition of mechanical damage presents a difficult problem. In this paper we shall avoid this delicate issue by refering to damage as simply a local reduction in material stiffness. Investigation of such phenomena is quite difficult, since knowledge of the microfailure criteria is incomplete and analytical results are usually restricted to academic simplifications. There are a variety of viewpoints to the general subject of damage: (1) atomistic (see reviews by Krajcinovic[3]), (2) thermodynamic, which attempt to relate micro/macro internal variables (see References 4 and 5) and (3) phemenological, which develop 'hereditary' laws, or history-type variables (see References 6–8). Rather than make an attempt to list the variety of approaches in the literature, we refer the reader to the exhaustive general survey found in Krajcinovic.[3] Obviously, the above approaches do not allow direct identification of the true damage in the material. In a sense, all the approaches are phemenological at one scale or the

* Correspondence to: P. Wriggers, Institut für Mechanik IV, Technische Universität Darmstadt, Hochschulstrasse1, D-64289 Darmstadt, Germany. E-mail: wriggers@newton.mechanik.th-darmstadt.de

CCC 0029–5981/98/030493–14$17.50

*Received 12 November 1997*
*Revised 4 March 1998*

other. Quantities such as dislocation density, void nucleation rate, etc., are extraordinarily difficult to measure, and virtually impossible to use in practical computations.

With this in mind, we present an approach, which is also phemenologically based, that accounts for damage in a material via unilateral constraints on the internal variables. If the constraints are violated, the material is forced to lose stiffness via a local reduction in the elasticity tensors eigenvalues. Therefore, the true damage is hidden in a local re-regularization of the material via a reduction of the material stiffness. By casting the damage process in this fashion it becomes easy to isolate a specific type of damage via a judicious choice of the constraints. However, since it is impossible to know *a priori* where, and if, the constraints are violated throughout the body, the problem is non-linear. Accordingly, a simple iterative algorithm is developed to solve this problem by (1) computing the internal fields with the initial undamaged microstructure and (2) reducing the material stiffness at locations where the constraints are violated. This process is repeated until the equations of equilibrium and the constraints are satisfied. For a given load, the microstructure at the end of the process is the 'damaged' microstructure.

The objective of this paper is to present the basic model, a general algorithm to solve it, and to provide some examples of where it is of possible benefit. A particularly important application, illustrated later, is the description of macroscopic damage in composite materials. The outline of the paper is as follows. In Section 2 the governing equations for the model are laid down. In Section 3 a general algorithm is presented. In Section 4 the finite element method, which plays a supporting role in examples, is discussed. Special attention is paid to issues of numerical accuracy and mesh dependency. In Section 5 the overall algorithm, in conjunction with the finite element method, is used to simulate the macroscopic damaged response of a widely used Aluminum–Boron composite combination. The results are compared to laboratory experiments published by Kyono *et al.*[1] and computational results using standard numerical methods published by Brockenbrough *et al.*[2] Finally, in Section 6 a summary is given.

## 2. GOVERNING EQUATIONS

We consider a structure composed of initially linearly elastic material which occupies an open bounded domain in $\Omega \in \mathbb{R}^3$. Its boundary is denoted $\partial\Omega$. The body is in static equilibrium under the action of body forces, $f(x)$, and surface tractions, $f(x)$. The boundary $\partial\Omega$ consists of a portion $\Gamma_u$ on which the displacements, $d(x)$, are prescribed, and a part $\Gamma_t$ on which tractions, $t(x)$, are prescribed. In this paper only infinitesmal strains are considered. From this point onward we drop the heavy $(x)$ notation, where it is clear that all quantities are a function of position unless explicitly otherwise stated.

### *2.1. Undamaged formulation*

We denote $\mathbf{u}^0$ as the 'undamaged' solution which is the solution of the following classical linear elastostatics problem:

$$\begin{aligned} -\nabla \cdot (\mathbf{E}^0 : \nabla \mathbf{u}^0) &= \mathbf{f}, \quad \forall \mathbf{x} \in \Omega \\ \mathbf{u}^0 &= \mathbf{d}, \quad \forall \mathbf{x} \in \Gamma_u \\ \mathbf{n} \cdot (\mathbf{E}^0 : \nabla \mathbf{u}^0) &= \mathbf{t}, \quad \forall \mathbf{x} \in \Gamma_t \end{aligned} \tag{1}$$

 

Here $\mathbf{E}^0$ is the fourth-order (undamaged) elasticity tensor with the usual symmetries and positive-definite character. $\mathbf{E}^0$ can be anisotropic with components that are functions of spatial position in the body.

### 2.2. Introduction of damage

The damaged solution, $\mathbf{u}^{\mathrm{D}}$, is characterized by the following

$$\boxed{\begin{aligned} -\nabla \cdot \mathbf{D}(\mathbf{u}^{\mathrm{D}}) &= \mathbf{f}, \quad \forall \mathbf{x} \in \Omega \\ \mathbf{u}^{\mathrm{D}} &= \mathbf{d}, \quad \forall \mathbf{x} \in \Gamma_u \\ \mathbf{n} \cdot \mathbf{D}(\mathbf{u}^{\mathrm{D}}) &= \mathbf{t}, \quad \forall \mathbf{x} \in \Gamma_t \end{aligned}} \tag{2}$$

$\mathbf{D}(\mathbf{u}^{\mathrm{D}})$ is spatially variable and non-linear, i.e. dependent on the solution, its gradient and possibly higher gradients in a non-linear fashion. There are obviously an infinite number of possible choices for the form of $\mathbf{D}(\mathbf{u}^{\mathrm{D}})$. In this paper we select $\mathbf{D}(\mathbf{u}^{\mathrm{D}})$ to be of a certain form (multiplicative decomposition, with constraints):

$$\boxed{\begin{aligned} &\mathbf{D}(\mathbf{u}^{\mathrm{D}}) \stackrel{\mathrm{def}}{=} (\mathbf{A}(\mathbf{u}^{\mathrm{D}}) : \mathbf{E}^0) : \nabla \mathbf{u}^{\mathrm{D}} \\ &\mathbf{0} < \mathbf{A}(\mathbf{u}^{\mathrm{D}}) < \mathbf{I} \text{ if } \boldsymbol{\phi}(\mathbf{u}^{\mathrm{D}}) = \mathbf{K} \text{ at } \mathbf{x} \\ &\mathbf{0} < \mathbf{A}(\mathbf{u}^{\mathrm{D}}) = \mathbf{I} \text{ if } \boldsymbol{\phi}(\mathbf{u}^{\mathrm{D}}) < \mathbf{K} \text{ at } \mathbf{x} \end{aligned}} \tag{3}$$

Here $\boldsymbol{\phi}(\mathbf{u}^{\mathrm{D}})$ serves as a functional which is used to measure selected internal fields of our choosing, for example the stress, strain, strain energy density, deviatoric energy, etc., and $\mathbf{K}$ serves as a constraint. The purpose of the tensorial damage variable $\mathbf{A}(\mathbf{u}^{\mathrm{D}})$ is to suppress selected internal variables, such as the stress field, below a critical level for a given external loading. The inequality $\mathbf{I} > \mathbf{A}(\mathbf{u}^{\mathrm{D}})$ means that the eigenvalues of $\mathbf{I} - \mathbf{A}(\mathbf{u}^{\mathrm{D}})$ are positive at a point.

One can interpret $\mathbf{A}(\mathbf{u}^{\mathrm{D}})$ as inducing a relaxation, or 'energy release' of the microstructure with progressive damage. It can, in general, be a scalar, vector or tensor function. The true micro-damage mechanisms could be any of a variety, depending on the type of material under analysis. For example damage mechanisms, such as microcracking, microvoid nucleation, dislocation growth or debonding, etc. could generate the stiffness reduction. Therefore, a judicious choice of $\boldsymbol{\phi}(\mathbf{u}^{\mathrm{D}})$ is necessary and should depend on the type of failure modes expected. Some obvious examples are $\boldsymbol{\phi}(\mathbf{u}^{\mathrm{D}}) = \boldsymbol{\sigma}$, $\boldsymbol{\phi}(\mathbf{u}^{\mathrm{D}}) = \boldsymbol{\sigma} : \boldsymbol{\varepsilon}$, etc. A more indepth discussion of the choice of the constraints will be given later in the paper.

## 3. A GENERAL SOLUTION ALGORITHM

In order to solve the constrained problem, a straightforward, and simple, algorithm is developed.

 

### *3.1. The algorithm*

As we have mentioned earlier, the basic idea is to (1) load the body with the initial linear elastic microstructure (2) compute a corresponding trial solution by solving the equations of equilibrium, (3) compute $\boldsymbol{\phi}(\mathbf{u}^{\text{trial}})$ at all point $\mathbf{x}$ in the body and (4) reduce the material stiffness where $\boldsymbol{\phi}(\mathbf{u}^{\text{trial}}) > \mathbf{K}$. The process is then repeated until the microstructure 'stabilizes'. The procedure of reducing the material stiffness at a point involves reducing the eigenvalues of the undamaged elasticity tensor $\mathbf{E}^0$ by an amount proportional to the constraint violation at the point. For purposes of clarity only, we present an algorithm for scalar (isotropic) damage ($\boldsymbol{\phi}(\mathbf{u}^{\text{trial}})$ and $\mathbf{K}$ are scalars). We use the following notation:

$$\alpha \mathbf{E}^0 \text{ means } \alpha \times (\lambda_1^0, \lambda_2^0, \lambda_3^0, \lambda_4^0, \lambda_5^0, \lambda_6^0) \tag{4}$$

where the $\lambda_i^0$'s are the eigenvalues of $\mathbf{E}^0$.

The algorithm is

$$\begin{aligned}
&\textit{For each } \mathbf{x},\ \mathbf{E}^{\text{trial}} = \mathbf{E}^0 \\
&(\spadesuit) \textit{Compute: } \nabla \cdot (\mathbf{E}^{\text{trial}} : \nabla \mathbf{u}^{\text{trial}}) = -\mathbf{f} \\
&\textit{For each } \mathbf{x} \Rightarrow \mathbf{E}^{\text{update}} = \frac{K}{\phi(\mathbf{u}^{\text{trial}})} \mathbf{E}^{\text{trial}} \\
&\textit{If } \mathbf{E}^{\text{update}} > \mathbf{E}^0 \textit{ at } \mathbf{x} \Rightarrow \mathbf{E}^{\text{update}} = \mathbf{E}^0 \textit{ at } \mathbf{x} \\
&\textit{If } \frac{\| \max\{\phi(\mathbf{u}^{\text{trial}}), K\} - K \|_{L^2(\Omega)}}{\|K\|_{L^2(\Omega)}} > \text{tol}_\phi \Rightarrow \mathbf{E}^{\text{trial}} = \mathbf{E}^{\text{update}} \textit{ for each } \mathbf{x} \Rightarrow \textit{go to } \spadesuit \\
&\textit{If } \frac{\| \max\{\phi(\mathbf{u}^{\text{trial}}), K\} - K \|_{L^2(\Omega)}}{\|K\|_{L^2(\Omega)}} \leqslant \text{tol}_\phi \Rightarrow \text{stop} \\
&\textit{For each } \mathbf{x} : \mathbf{D} = \mathbf{E}^{\text{trial}},\ \mathbf{u}^{\text{D}} = \mathbf{u}^{\text{trial}} \ (\textit{final 'damaged' microstructure})
\end{aligned} \tag{5}$$

We use the standard norm: $\| \cdot \|^2_{L^2(\Omega)} \stackrel{\text{def}}{=} \int_\Omega (\cdot)^2 \, d\mathbf{x}$. The motivation of such an algorithm is clear. Ideally, after weakening the microstructure, if we were to reapply the same loading intensity to the updated microstructure, there should be no values of the internal variable throughout the body above the critical value. One can consider such a microstructure as macroscopically stable, since it ceases to change in a global $L^2(\Omega)$ norm.

### *3.2. Application to macroscopic "damaged" properties*

A basic theme in the analysis of structural materials has been to determine a damage dependent macroscopic response function, $\mathbf{D}^*$, from a relation between volumetric averages, over a statistically representative volume element (RVE), $\langle \boldsymbol{\sigma} \rangle = \mathbf{D}^*(\langle \boldsymbol{\varepsilon} \rangle)$, $\langle \cdot \rangle \stackrel{\text{def}}{=} (1/|\Omega|) \int_\Omega d\mathbf{x}$. Here $\boldsymbol{\sigma}$ and $\boldsymbol{\varepsilon}$ are the computed microstress and microstrain fields within the RVE domain, $\Omega$. For the RVE to be statistically representative, it usually must contain a significant amount of microstructure. This

 

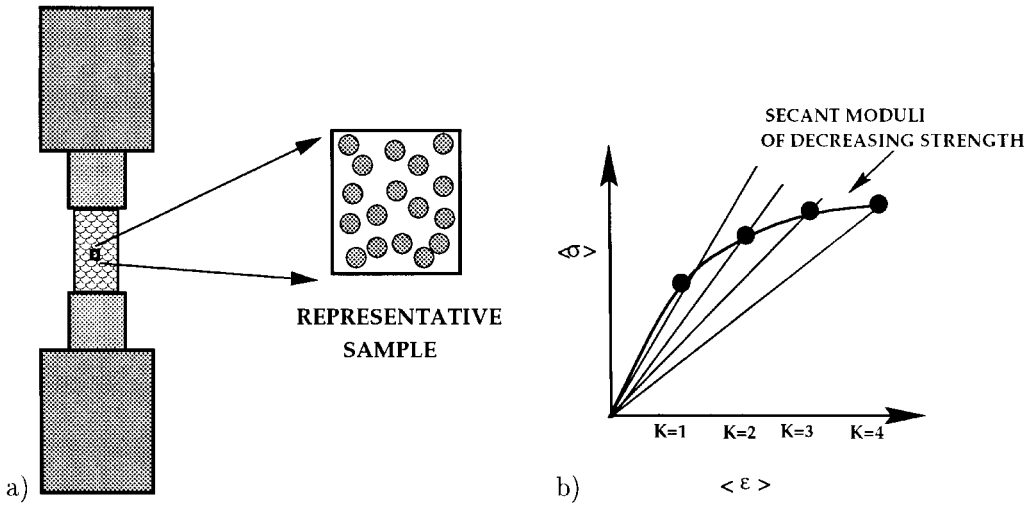


Figure 1. (a) The model problem; (b) succesive reduction of the secant moduli

fact usually makes computational algorithms and damage laws associated with these problems rather complex. An important application of the method introduced in this paper is to study the macroscopic damaged behaviour of a sample of composite material. The obvious goal is to determine the reduction of macroscopic stiffness with increasing loads. In order to make a coherent attempt to simulate the damaged response of a composite material we first briefly review the linear theory, which can be interpreted as a single incremental load step in the determination of $\mathbf{D}^*$.

*3.2.1. Background*

To determine an effective macroscopic linear elasticity tensor, $\mathbf{E}^*$, a relation between averages, $\langle\boldsymbol{\sigma}\rangle = \mathbf{E}^* : \langle\boldsymbol{\varepsilon}\rangle$, must be computed, where $\langle\cdot\rangle \stackrel{\text{def}}{=} (1/|\Omega|)\int_\Omega \mathrm{d}\mathbf{x}$, and where $\boldsymbol{\sigma}$ and $\boldsymbol{\varepsilon}$ are the stress and strain tensor fields within statistically representative volume element (RVE) with volume $|\Omega|$. Loosely speaking, an RVE is a theoretical structure that is small enough that it can be considered as a material point with respect to the size of the domain under analysis, but large enough to be a statistically representative sample of the microstructure (Figure 1). Here we assume that at least one choice of the RVE is possible. For details see Reference 9. The fact that the RVE must be statistically representative, makes computations, of even an undamaged material response, extremely complex and costly. This occurs primarily because, when employing numerical methods, such as the finite element, the distance between discretization nodes must be far smaller than the microstructural oscillations to obtain accurate simulations. This has made, until relatively recently, direct numerical simulations involving the real microstructure of the material virtually impossible for general macroscopic structures.

In general, $\mathbf{E}^*$ is not a material property, i.e. it is a relation between averages. For the general three dimensional anisotropic response, the usual procedure is to specify a set of six linearly independent loadings on the RVE boundary, either of uniform strain or uniform stress type. Each loading state provides explicit computation of six components of $\mathbf{E}^*$. Explicitly, one specifies 6 linearly independent loadings (in the three-dimensional case) of the form, (1) $\mathbf{u}|_{\partial\Omega} = \mathbf{S}\cdot\mathbf{x}$ *or* (2) $\mathbf{t}|_{\partial\Omega} = \mathbf{T}\cdot\mathbf{n}$ where $\mathbf{S}$ and $\mathbf{T}$ are symmetric second order strain and stress tensors, with constant components.

 

Each independent loading state provides six equations, for a total of 36, which are used to determine the relation between average stress and strain

$$\begin{bmatrix} \langle\sigma_{11}\rangle \\ \langle\sigma_{22}\rangle \\ \langle\sigma_{33}\rangle \\ \langle\sigma_{12}\rangle \\ \langle\sigma_{23}\rangle \\ \langle\sigma_{13}\rangle \end{bmatrix} = \begin{bmatrix} E^*_{1111} & E^*_{1122} & E^*_{1133} & E^*_{1112} & E^*_{1123} & E^*_{1113} \\ E^*_{2211} & E^*_{2222} & E^*_{2233} & E^*_{2212} & E^*_{2223} & E^*_{2213} \\ E^*_{3311} & E^*_{3322} & E^*_{3333} & E^*_{3312} & E^*_{3323} & E^*_{3313} \\ E^*_{1211} & E^*_{1222} & E^*_{1233} & E^*_{1212} & E^*_{1223} & E^*_{1213} \\ E^*_{2311} & E^*_{2322} & E^*_{2333} & E^*_{2312} & E^*_{2323} & E^*_{2313} \\ E^*_{1311} & E^*_{1322} & E^*_{1333} & E^*_{1312} & E^*_{1323} & E^*_{1313} \end{bmatrix} \begin{bmatrix} \langle\varepsilon_{11}\rangle \\ \langle\varepsilon_{22}\rangle \\ \langle\varepsilon_{33}\rangle \\ 2\langle\varepsilon_{12}\rangle \\ 2\langle\varepsilon_{23}\rangle \\ 2\langle\varepsilon_{13}\rangle \end{bmatrix} \tag{6}$$

We note that $\mathbf{E}^*$ is symmetric and has really only 21 independent constants in the general anisotropic case. The usual choices for the six independent load cases are

$$\mathbf{S} \text{ or } \mathbf{T} = \begin{bmatrix} \beta & 0 & 0 \\ 0 & 0 & 0 \\ 0 & 0 & 0 \end{bmatrix}, \begin{bmatrix} 0 & 0 & 0 \\ 0 & \beta & 0 \\ 0 & 0 & 0 \end{bmatrix}, \begin{bmatrix} 0 & 0 & 0 \\ 0 & 0 & 0 \\ 0 & 0 & \beta \end{bmatrix}, \begin{bmatrix} 0 & \beta & 0 \\ \beta & 0 & 0 \\ 0 & 0 & 0 \end{bmatrix}, \begin{bmatrix} 0 & 0 & 0 \\ 0 & 0 & \beta \\ 0 & \beta & 0 \end{bmatrix}, \begin{bmatrix} 0 & 0 & \beta \\ 0 & 0 & 0 \\ \beta & 0 & 0 \end{bmatrix}, \tag{7}$$

where $\beta$ is a load parameter.

### 3.3. Incorporation into a macroscopic effective damage algorithm

To determine the progressive damaged response of a composite material sample, essentially the algorithm in Box 5 is applied at each load increment. For example, for displacement controlled tests we have

*Step* I: *Partition loading*: $\Delta\beta \overset{\text{def}}{=} \frac{\beta}{N}$

*Step* II: *Apply load increment*: $\mathbf{u}^{(L)}|_{\partial\Omega} \overset{\text{def}}{=} L \times \Delta\beta \cdot \mathbf{x},\ L = 1, 2..N.$

*Step* III: *Use* $\mathbf{E}^{(L-1)}$ *as the undamaged microstructure* ($L = 1$ *initially*)

*Step* IV: *Apply damage algorithm for* $\mathbf{u}^{(L)}|_{\partial\Omega}$ (8)

*Step* V: *Store stablized damaged microstructure* $\Rightarrow \mathbf{E}^{(L)}$ *and solution* $\mathbf{u}^{(D,L)}$

*Step* VI: *Goto Step* II *and repeat for next load increment with* $L = L + 1$

*Step* VII: *Post process* $\mathbf{E}^{(L)}\ L = 1, 2, \ldots, N \Rightarrow \langle\boldsymbol{\sigma}^{(D,L)}\rangle = \mathbf{E}^{*(L)} : \langle\boldsymbol{\varepsilon}^{(D,L)}\rangle.$

The end result is a series of effective *secant* moduli, $\mathbf{E}^{*(L)},\ L = 1, 2, \ldots, N$, that can be thought of, collectively, as representing the macroscopic damaged response $\mathbf{D}^*$. The process is essentially the same for traction controlled tests.

 

## 4. NUMERICAL DISCRETIZATION

A central interest is to simulate damage in composite materials. The algorithm presented must be used in conjunction with a numerical method, for example, the finite element method. Accordingly, for reliable numerical accuracy in the simulations, a primary computational concern is to determine an adequate mesh density to capture the evolving damaged microstructure. There are essentially two choices to mesh the microstructure with the finite element method, an 'Eulerian' or a 'Lagrangian' approach. An Eulerian approach does not require the finite element boundaries to align with material boundaries when meshing the internal geometry. A Lagrangian approach would impose that the element boundaries coincide with material interfaces and therefore the elements have no material dicontinuities within them. For more details on meshing approaches see Zukas *et al.*[10] for a general discussion of the two approaches. In order to get a feeling for the relative behaviour of the two approaches we compare Eulerian and Lagrangian meshing approaches, for the same number of degrees of freedom, for a simple set of examples. We use bilinear shape functions. Since we use a numerical method based on energy-based principles (finite element method) to generate solutions, it is natural to measure differences between the two meshing techniques via their strain energies.

Numerical tests were performed on a widely used Aluminum/Boron fibre-reinforced composite combination. The material chosen is a 6061 Aluminum-o alloy reinforced with 46 per cent Boron unidirectional fibres. The material data is taken from Kyono *et al.*[1] and is shown in Table I. This material is also used in larger experiments in the next section. We consider two-dimensional plane strain conditions. The meshes are shown in Figure 3 and the numerical results in Table II. Higher quadrature rules above the canonical usage are also employed within the finite elements for the Eulerian meshing case to more accurately capture any discontinuities within the finite elements (although never higher than $4 \times 4$ Gauss rules). Uniaxial tension was applied.

Comparing the strain energies, these results, which were representative of others performed, imply that above approximately 64–256 elements/fibre, in 2-D, we have relatively accurate results,

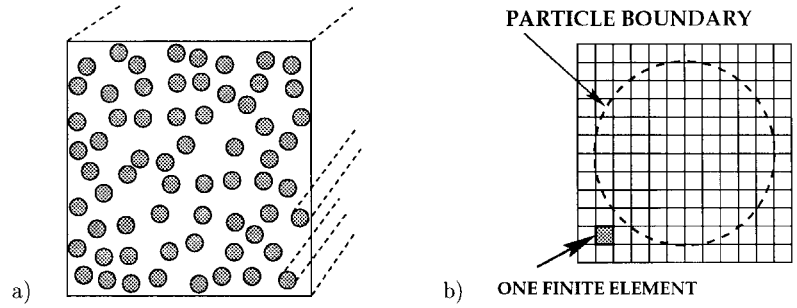


Figure 2. (a) The microstructure; (b) a blowup of a typical finite element mesh used in the numerical calculations

Table I. Material data for the composite simulation

| Material | Vol. frac. (%) | $\kappa$ (GPa) | $\mu$ (GPa) |
|---|---|---|---|
| FIBRE:Boron | 46 | 230 | 172 |
| MATRIX:6061 Aluminum | 54 | 67·5 | 25·9 |

 

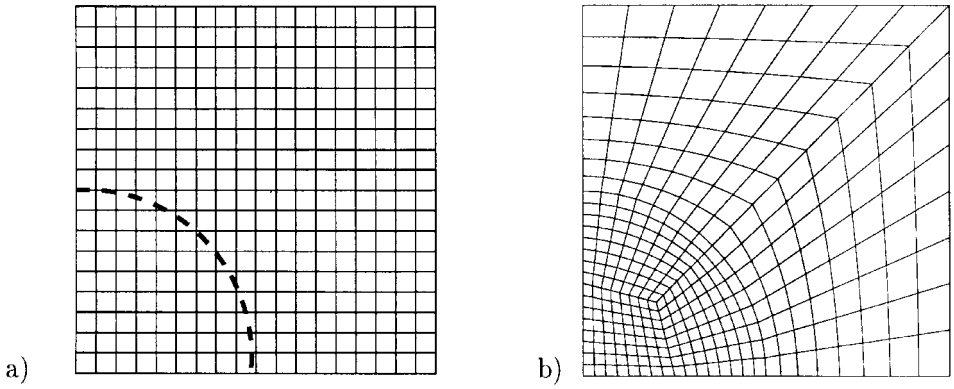


Figure 3. One-quarter of the meshes used for a single fibre with: (a) Eulerian meshing; and (b) Lagrangian meshing

Table II. A comparison between Eulerian and Lagrangian meshing

| full mesh | $8 \times 8 = 64$ | $12 \times 12 = 144$ | $16 \times 16 = 256$ | $20 \times 20 = 400$ |
|---|---|---|---|---|
| $\frac{\lvert U^{\text{lag}} - U^{\text{eul}} \rvert}{\lvert U^{\text{lag}} \rvert}$ | 3·42 per cent | 2·83 per cent | 1·95 per cent | 1·77 per cent |

i.e. 1·77 per cent $\leqslant \frac{|U^{\text{lag}} - U^{\text{eul}}|}{|U^{\text{lag}}|} \leqslant$ 3·42 per cent, where

$$\frac{|U^{\text{eul}} - U^{\text{lag}}|}{|U^{\text{lag}}|} \stackrel{\text{def}}{=} \frac{\left| \left( \int_\Omega \nabla \mathbf{u}^{h_{\text{eul}}} : \mathbf{E} : \nabla \mathbf{u}^{h_{\text{eul}}} \, \mathrm{d}\mathbf{x} \right) - \left( \int_\Omega \nabla \mathbf{u}^{h_{\text{lag}}} : \mathbf{E} : \nabla \mathbf{u}^{h_{\text{lag}}} \, \mathrm{d}\mathbf{x} \right) \right|}{\int_\Omega \nabla \mathbf{u}^{h_{\text{lag}}} : \mathbf{E} : \nabla \mathbf{u}^{h_{\text{lag}}} \, \mathrm{d}\mathbf{x}}. \tag{9}$$

We note that the Lagrangian solution was stable using approximately 400 elements, and the corresponding solution can be taken as essentially 'exact'. For other loadings, such as shear loading, the results are essentially identical. For simplicity, and to consider a somewhat complicated realistic microstructure (for example, multiple interacting fibres), for the remainder of this paper we opt for a Eulerian meshing approach.

To control the absolute error for the Eulerian approach, for multiple particles, the simplest, of error estimation techniques, based on extrapolation, is used. The standard *a priori* error estimate for the finite element method is

$$\|\mathbf{u} - \mathbf{u}^h\|_{E(\Omega)} \leqslant \mathscr{C}(\mathbf{u}, p) h^{\min(s-1,p)} \stackrel{\text{def}}{=} w, \quad \|\mathbf{u} - \mathbf{u}^h\|^2_{E(\Omega)} = \int_\Omega \nabla(\mathbf{u} - \mathbf{u}^h) : \mathbf{E} : (\mathbf{u} - \mathbf{u}^h) \, \mathrm{d}\mathbf{x} \tag{10}$$

where $p$ is the polynomial order of the finite element method used, $s$ is the regularity of the exact solution, $\mathscr{C}$ is a constant dependent on the exact solution and the polynomial approximation, but independent of $h$ (the maximum element diameter). Typically, for the class of problems of interest, the true solution is not smooth due to the initial material interfaces in the undamaged material and the evolving damage fronts. In this case, the rate of convergence is essentially in the

 

following range: $1 < s \leqslant \frac{3}{2}$. Therefore, because of the low regularity of the true solution, we use the $h$-version finite element method (with bilinear shape functions) which is based on successive mesh subdivision. We utilize the following relations to estimate the premultiplicative constant $\mathscr{C}$:

$$\|\mathbf{u} - \mathbf{u}^{h_1}\|^2_{E(\Omega)} \leqslant \mathscr{C}^2(\mathbf{u}, p) h_1^{2w}$$

$$\|\mathbf{u} - \mathbf{u}^{h_2}\|^2_{E(\Omega)} \leqslant \mathscr{C}^2(\mathbf{u}, p) h_2^{2w}, \quad h_1 < h_2$$

$$\|\mathbf{u} - \mathbf{u}^{h}\|^2_{E(\Omega)} = 2(\mathscr{J}(\mathbf{u}^h) - \mathscr{J}(\mathbf{u}))$$

$$\mathscr{J}(\mathbf{u}) \stackrel{\text{def}}{=} \frac{1}{2}\int_\Omega \nabla \mathbf{u} : \mathbf{E} : \nabla \mathbf{u}\, \mathrm{d}\mathbf{x} - \int_\Omega \mathbf{f} \cdot \mathbf{u}\, \mathrm{d}\mathbf{x} - \int_{\Gamma_t} \mathbf{t} \cdot \mathbf{u}\, \mathrm{d}s.$$

Using these relations and assuming that $\mathscr{J}(\mathbf{u}^{h_2}) \leqslant \mathscr{J}(\mathbf{u}^{h_1})$, which is a natural consequence of the Principle of Minimum Potential Energy yields

$$\mathscr{C}^2 \approx \frac{2\mathscr{J}(\mathbf{u}^{h_1}) - 2\mathscr{J}(\mathbf{u}^{h_2})}{h_1^{2w} - h_2^{2w}} \tag{11}$$

We then specify $e^{\text{target}}$ and solve for the required mesh size

$$e^{\text{target}} \stackrel{\text{def}}{=} \frac{\|\mathbf{u} - \mathbf{u}^{h_{\text{tol}}}\|_{E(\Omega)}}{\|\mathbf{u}^{h_{\text{tol}}}\|_{E(\Omega)}} \approx \frac{C h_{\text{tol}}^w}{\|\mathbf{u}^{h_{\text{tol}}}\|_{E(\Omega)}} \Rightarrow h_{\text{tol}} \approx \left(\frac{e^{\text{target}} \|\mathbf{u}^{h_{\text{tol}}}\|_{E(\Omega)}}{\mathscr{C}}\right)^{1/w} \tag{12}$$

This was used as a guide in the following manner:

*Step* 1 : *Compute* $\mathscr{C}$ *from two succesive mesh densities* ($4 \times 4$ *and* $8 \times 8$):

$$\mathscr{C} \approx \sqrt{\frac{2\mathscr{J}(\mathbf{u}^{h_1}) - 2\mathscr{J}(\mathbf{u}^{h_2})}{h_1 - h_2}}$$

*Step* 2 : *Estimate the needed mesh density for a target error* (13)

$$h_{\text{tol}} \approx \left(\frac{e^{\text{target}} \|\mathbf{u}^{h_{\text{tol}}}\|_{E(\Omega)}}{\mathscr{C}}\right)^{1/w}$$

*Step* 3 : *To check* : *Repeat the procedure with higher mesh density*

Typically, for error under 2 per cent, a mesh density between $12 \times 12$ and $16 \times 16$, *per particle*, was needed.

## 5. SIMULATION OF AN ALUMINUM/BORON COMPOSITE

Numerical tests, using the algorithm, were performed on a widely used Aluminum/Boron fiber-reinforced composite combination. The material chosen is a 6061 Aluminum-o alloy reinforced with

 

46 per cent Boron unidirectional fibers. The primary source for damage in the material is in the ductile Aluminum matrix. Random placement of the fibre cross-sections are given in the transverse plane. The effective moduli of such an arrangement is approximately transversely isotropic. We considered a sequence of microstructures $1 \times 1$, $2 \times 2$, $4 \times 4$, etc. fiber arrangements (randomly positioned) until we measured no more change in 3 successive effective properties (under one-half of one percent). For this specific microstructure this occurred starting with the sequence $8 \times 8$, $12 \times 12$, $16 \times 16$. The tests in this experiment are 'uniform' boundary loading of the form:

$$\mathbf{u}|_{\partial\Omega} = \mathscr{S} \cdot \mathbf{x} \text{ where } \mathscr{S} = \begin{bmatrix} S_{11} & S_{21} & S_{31} \\ S_{12} & S_{22} & S_{32} \\ S_{13} & S_{23} & S_{33} \end{bmatrix} = \begin{bmatrix} 0 & 0 & 0 \\ 0 & S_{22} & 0 \\ 0 & 0 & 0 \end{bmatrix} \tag{14}$$

### *5.1. Choice of a constraint*

The selection of $\mathbf{K}$ and $\boldsymbol{\phi}$ should be made to isolate the damage mechanism of interest in the simulation. For this particular composite combination it is ductile failure in the matrix. Therefore the constraint should be selected with this in mind. To show a relation of the formulation to plasticity formulations $\mathbf{K}$ and $\boldsymbol{\phi}(\mathbf{u}^{\mathrm{D}})$ would be selected as follows:

$$\mathbf{K} = \sigma^{\bigstar} + H\varepsilon_{\mathrm{eq}}^{\mathrm{in}}, \quad \boldsymbol{\phi} = \sqrt{\tfrac{3}{2}\mathbf{s} : \mathbf{s}} \tag{15}$$

where $\sigma^{\bigstar}$ and $H$ are fixed, denoting the one-dimensional initial yield stress and isotropic linear hardening modulus, respectively. $\mathbf{s}$ is the deviatoric stress and $\varepsilon_{\mathrm{eq}}^{\mathrm{in}}$ is the local equivalent inelastic strain for the material at point $\mathbf{x}$. It is emphasized that, in contrast to conventional plasticity, $\varepsilon_{\mathrm{eq}}^{\mathrm{in}}$ is not a history variable. It is calculated only with knowledge of the actual microfield quantities:

$$\varepsilon_{\mathrm{eq}}^{\mathrm{in}} = \sqrt{\tfrac{2}{3}\mathbf{e}^{\mathrm{in}} : \mathbf{e}^{\mathrm{in}}}, \quad \varepsilon^{\mathrm{in}} = \varepsilon - (\mathbf{E}^{0})^{-1} : \boldsymbol{\sigma} \tag{16}$$

where $\mathbf{E}^{0}$ denotes the initial undamaged material stiffness and $\mathbf{e}^{\mathrm{in}}$ the inelastic deviatoric strain. Obviously, this selection of $\mathbf{K}$ and $\boldsymbol{\phi}(\mathbf{u}^{\mathrm{D}})$ has a character close to conventional elastoplasticity. We briefly illustrate the similarities and the differences. The well-known von Mises flow function, including linear isotropic work hardening reads as follows:

$$\boldsymbol{\phi}(\boldsymbol{\sigma}) = \sqrt{\mathbf{s} : \mathbf{s}} - \sqrt{\tfrac{2}{3}}(\sigma^{\bigstar} + H\varepsilon_{\mathrm{eq}}^{\mathrm{pl}}) \tag{17}$$

We use the associated flow rule for the plastic strain increment

$$\Delta\varepsilon^{\mathrm{pl}} = \Delta\gamma \frac{\partial \boldsymbol{\phi}}{\partial \mathbf{s}} \tag{18}$$

and we define the elastic trial state, which is obtained by 'freezing' the plastic flow. Then we can solve for the unknown Lagrange multiplier $\Delta\gamma$ by enforcing fulfillment of the consistency condition at the end of the actual load increment (see Reference 11 for details), obtaining

$$\Delta\gamma = \frac{\sqrt{\mathbf{s}^{\mathrm{trial}} : \mathbf{s}^{\mathrm{trial}}} - \frac{2}{3}(\sigma^{\bigstar} + H\varepsilon_{\mathrm{eq}}^{\mathrm{pl}})}{2\mu + \frac{2}{3}\kappa} \tag{19}$$

The stress is then computed

$$\boldsymbol{\sigma} = \kappa \operatorname{tr} \varepsilon \mathbf{I} + 2\mu(\mathbf{e} - \mathbf{e}^{\mathrm{pl}}) \tag{20}$$

 

with $\kappa, \mu$ being bulk and shear modulus, and $\mathbf{e}$ the strain deviator, respectively. Now, we define the same stress state, but assuming that there is no plastic strain, therefore the elastic constants must be altered to

$$\boldsymbol{\sigma} = \hat{\kappa}\,\mathrm{tr}\,\varepsilon\mathbf{I} + 2\hat{\mu}(\mathbf{e}) \tag{21}$$

If we assume further that plasticity only affects the shear modulus ($\kappa = \hat{\kappa}$), as it is usually done in metal plasticity, then it follows

$$2\hat{\mu}\mathbf{e} = 2\mu(\mathbf{e} - \Delta\mathbf{e}^{\mathrm{pl}}) \tag{22}$$

Taking the inner product both sides with $\mathbf{e}$ and dividing by $\mu$ yields

$$\frac{\hat{\mu}}{\mu} = \frac{\mathbf{e}\cdot\mathbf{e} - \mathbf{e}\cdot\Delta\mathbf{e}^{\mathrm{pl}}}{\mathbf{e}\cdot\mathbf{e}} \tag{23}$$

and after some algebra

$$\frac{\hat{\mu}}{\mu} = \frac{H}{3\mu + H} + \frac{2\mu}{2\mu + \frac{2}{3}H}\frac{\sigma^{\bigstar} + H\varepsilon_{\mathrm{eq}}^{\mathrm{pl}}}{\sqrt{\frac{3}{2}\mathbf{s}^{\mathrm{trial}} : \mathbf{s}^{\mathrm{trial}}}} \tag{24}$$

Therefore, selecting $\boldsymbol{\phi} = \sqrt{\frac{3}{2}\mathbf{s} : \mathbf{s}}$ would force the formulation to coincide exactly, if we define $A\mu = \hat{\mu}$, $(\mathbf{A}(\mathbf{u}^{\mathrm{D}}) : \mathbf{E}^0 = \mathbf{D})$. Only in the case where the material is isotropic, the bulk modulus is never altered, with no work hardening will the algorithm coincide with classical elastoplasticity, otherwise they are different.

If the material is isotropic then the eigenvalues are

$$\mathrm{Eig}(\mathbf{E}^0) = \{3\kappa^0, 2\mu^0, 2\mu^0, \mu^0, \mu^0, \mu^0\} \tag{25}$$

and for the locations where there are violations:

$$\kappa^{\mathrm{update}} = \frac{K}{\phi(\mathbf{u}^{\mathrm{D}})}\kappa^{\mathrm{trial}}, \quad \mu^{\mathrm{update}} = \frac{K}{\phi(\mathbf{u}^{\mathrm{D}})}\mu^{\mathrm{trial}} \tag{26}$$

where the complete isotropic elasticity tensor is given by

$$\mathbf{E} \overset{\mathrm{def}}{=} \begin{bmatrix} \kappa + \frac{4}{3}\mu & \kappa - \frac{2}{3}\mu & \kappa - \frac{2}{3}\mu & 0 & 0 & 0 \\ \kappa - \frac{2}{3}\mu & \kappa + \frac{4}{3}\mu & \kappa - \frac{2}{3}\mu & 0 & 0 & 0 \\ \kappa - \frac{2}{3}\mu & \kappa - \frac{2}{3}\mu & \kappa + \frac{4}{3}\mu & 0 & 0 & 0 \\ 0 & 0 & 0 & \mu & 0 & 0 \\ 0 & 0 & 0 & 0 & \mu & 0 \\ 0 & 0 & 0 & 0 & 0 & \mu \end{bmatrix} \tag{27}$$

We now compare laboratory experiments, numerical solutions produced by conventional elasto-plasticity, and the solution produced by the algorithm presented in this paper.

 

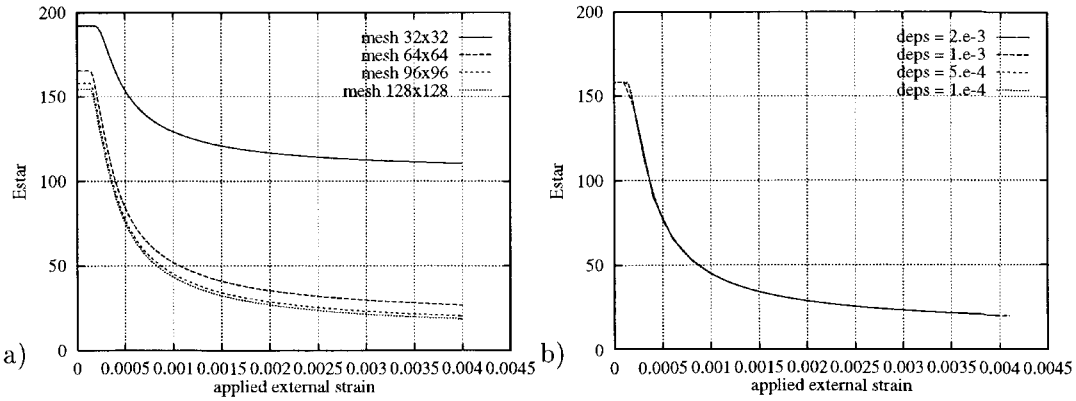


Figure 4. The evolution of $E_y^* =$ effective Young's modulus versus the load: (a) for different (total) meshes and fixed load increment; (b) for various load increments and fixed mesh

### 5.2. *Results*

We use the loading in relation (14). We compared our results with a (1) previous numerical study of Brockenbrough, Suresh and Wienecke[2] who used conventional elastoplasticity, and (2) experimental results of Kyono *et al.*[1] We assume that the Boron fibres remain linear elastic and perfectly bonded to the 6061 Aluminum matrix (as in Reference 2). The assumption of perfect bonding is known to be reasonable for this material (see Reference 12 for details). We use the relations in equation (15) for the ductile Aluminum-o matrix with $\sigma^{\star} = 22{\cdot}5$ MPa and $H = 2{\cdot}5$ GPa.

Clearly, all quantities, which are post-processed from the microfield are mesh dependent, however, they stabilize beyond a certain mesh threshhold. For this example, the threshhold was usually between $144(12 \times 12) - 256(16 \times 16)$ elements *per fibre* for a total between 18 818–33 282 unknowns. The interpretation of the behaviour of $E_y^*$ with increasing $\mathscr{S}_{22}$ (Figure 4(a)) is straightforward. The simulations were also repeated for increasing smaller load increments ($0{\cdot}002 \rightarrow 0{\cdot}0001$ strain) as shown in Figure 4(b) with the highest mesh density. It is clear that as the material is progressively damaged, it tends to a more homogeneous state. For this test the general trend is

$$0{\cdot}3489\mathscr{S}_{22}^{-0{\cdot}7177} \approx D_y^* \quad \text{(Damaged Young's modulus)} \tag{28}$$

where the regression value of the curve fit is $R^2 = 0{\cdot}99$. We note that $R^2 = 1{\cdot}00$ is a perfect curve fit. Figure 4 indicates after initial macroscopic 'yielding', the material stabilizes, and the response is that of a much weaker material. Figures 5(a) and 5(b) illustrate the predicted relation between macroscopic stress and strain, which is in close agreement with the experimental work published by Kyono *et al.*[1] Also the curves are in agreement with numerical results using the finite element method, published by Brockenbrough *et al.*[2] who modelled the 6061 Aluminum-o matrix as an isotropic hardening elasto-plastic solid, using conventional numerical methods. The results in Brockenbrough *et al.*[2] coincide at the experimental points. The curve asserts that after yielding the macroscopic response is linear and only slightly stiffer than the 6061 Aluminum matrix alone. Essentially, 'plastic plugs' envelope the Boron fibres after excessive yielding and, consequently, their contribution to the stiffness becomes negligible.

 

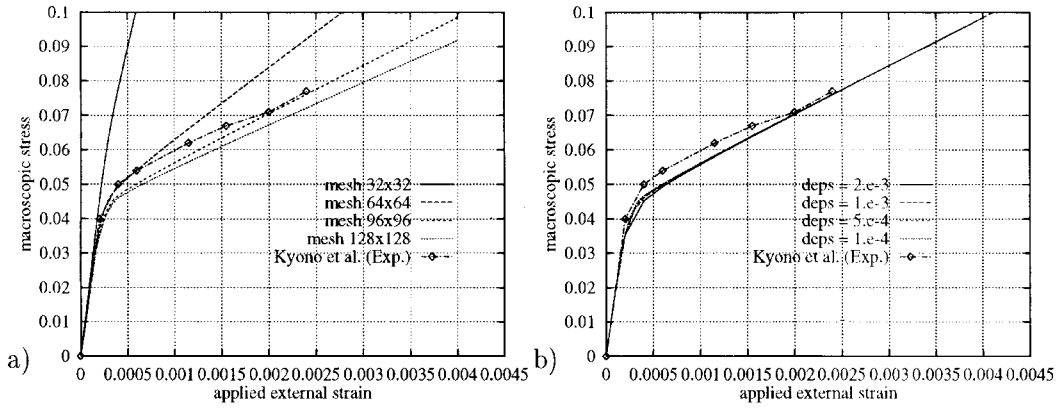


Figure 5. The evolution of $\langle \sigma_{22} \rangle$ versus the load: (a) for different meshes and fixed load increment; (b) for various load increments and fixed mesh

## 6. SUMMARY

To an extent, this is still work in progress. However, there are some concluding observations at this point in the research. Since the iterative algorithm used to solve the model's governing equations involves solving a linear elasticity problem at each stage, it is amenable to standard error estimators and domain decomposition techniques. This is an important point, since the numerical performance of many methods, which are successful on two-dimensional problems, degrade rapidly when applied to three-dimensional problems due to increased memory and computational requirements. As one example the method was applied to a Aluminum/Boron composite. The good agreement of the numerical results with experiments indicates the potential of the approach. It is important to emphasize that the method is independent of any numerical discretization technique. We have used the finite element method out of convenience.

A critical point to emphasize is that $\boldsymbol{\phi}(\mathbf{u}^{\mathrm{D}})$ and $\mathbf{K}$ have no *a priori* smoothness or continuity requirements. Indeed they can be discontinuous, and, in fact, it is advantageous to design them to be so. For example, a rather obvious choice illustrating this is interfacial debonding. In this case the constraint should be selected to reflect an interfacial debonding limit and $\mathbf{K}$ could be selected as follows:

$$\mathbf{K} = \begin{cases} \sigma^{\mathrm{I}} & \text{if } \mathbf{x} \in \text{interface} \\ \infty & \text{if } \mathbf{x} \notin \text{interface} \end{cases} \qquad \boldsymbol{\phi}(\mathbf{u}^{\mathrm{D}}) \stackrel{\text{def}}{=} \boldsymbol{\sigma} < \mathbf{K} \quad \forall \mathbf{x} \in \Omega \tag{29}$$

where $\sigma^{\mathrm{I}}$ is the interface stiffness of the material. In the general algorithm the internal variables used in the local damage model have been purposely left arbitrary, making the method flexible enough to accomodate a variety of materials including different microdamage mechanisms. This could be an interesting issue in future investigations, involving microcracking in brittle solids. In particular, this would involve the possible selection of $\boldsymbol{\phi} = J_1$-integral which is the energy release rate (see References 13 or 14 or 15) criteria valid for brittle fracture.

ACKNOWLEDGEMENT

The authors wish to thank Stefan Löhnert for his help in the computations presented in Section 4.

 

REFERENCES

1. T. Kyono, W. Hall and M. Taya, *ASTM STP*, **964,** 409–431 (1986).
2. S. Brockenbrough, S. Suresh and H. A. Wienecke, *Acta Metall. Mater.*, **39,** 735–752 (1991).
3. D. Krajcinovic, *Damage Mechanics*, North-Holland, Amsterdam, 1996.
4. J. Kestin and J. R. Rice, 'Paradoxes in the application of thermo-dynamics to strained solids', in E. B. Stuart, B. Gal Or and A. J. Brainard (eds.), *A Critical Review of Thermodynamics*, Mono-Book Corp., Baltimore, MD, 1970, pp. 275–298.
5. R. Hill and J. R. Rice, 'Elastic potentials and the structure of inelastic constitutive laws', *SIAM J. Appl. Math*., **25,** 448–461 (1973).
6. J. Lemaitre and J.-L. Chaboche, *Mechanics of Solid Material*, Cambridge University Press, Cambridge, 1990.
7. J. Lemaitre, 'Coupled elasto-plasticity and damage constitutive equations', *Comput. Meth. Appl. Mech. Engng.*, **51,** 31–49 (1985).
8. P. Ladaveze, A. Gasser and O. Allix, 'Damage modeling for ceramic composites', *J. Engng. Mat. Tech.*, **116,** 331–336 (1994).
9. P. Suquet, 'Elements of homogenization for inelastic solids', in E. Sanchez-Palencia and A. Zaoui (eds.), *Homogenization Techniques for Composite Media*, Lecture Note in Physics, vol. 272, Springer, Berlin, 1987, pp. 193–278.
10. J. Zukas, T. Nicholas, H. Swift, L. B. Greszczuk and D. Curran, *Impact Dynamics*, Wiley, New York, 1982.
11. J. C. Simo, *Topics on the Numerical Analysis and Simulation of Plasticity*, Elsevier Science, 1998, to appear.
12. H. J. Böhm and F. G. Rammersdorfer, *Mater. Sci. Engng.*, **A135,** 185–190 (1991).
13. G. P. Cherepanov, 'Crack propagation in continuous media', *USSR J. Appl. Math. Mech. Transl.*, **31,** 504 (1967).
14. J. Rice, 'A path independent integral and the approximate analysis of strain concentration by notches and cracks', *J. Appl. Mech.*, 379–386 (1968).
15. A. Griffith, 'The phenomena of rupture flow in solids', *Phil. Trans. Roy. Soc. London*, **A221,** 163–197 (1921).
16. L. M. Kachanov, *Introduction to Continuum Damage Mechanics*, Martinus Nijoff, Dordrecht, 1986.

 